JOURNAL OF THERMOPHYSICS AND HEAT TRANSFER
Vol. 24, No. 2, April–June 2010

Thermal Fluid Process in a Small Universal Electric Motor

Hongmin Li*
ECR International, Utica, New York 13504

DOI: 10.2514/1.43641

This paper presents an investigation of the heat transfer and fluid flow process in a small universal electric motor, which employs a stamped metal axial flow cooling fan. A three-dimensional conjugate computational model is developed. An experimental testing system is built to measure the flow rates of cooling air at various rotation speeds. The agreement between the experimental data and the model predictions is reasonably good. The numerical approach presents detailed flow structures, temperature distributions, and quantitative heat flux data. The cooling flowpath, heat transfer process, and the fluid driving of the cooling fan are analyzed. Suggestions for universal motor development and cooling design are given.

Nomenclature

A_A = total armature surface area, m^2
a_s = speed of sound
C_p = specific heat, J/kg/°C
E = enthalpy, J
E_g = heat generation per unit volume, W/m^3
$\mathbf{g}$ = gravity vector
H_F = air film thickness, mm
h_{av} = average convection coefficient, $W/m^2/°C$
h_S = solid enthalpy, J/kg/°C
I = electrical current, A
K_S = solid conductivity, W/m/°C
k_{eff} = effective conductivity, W/m/°C
M = cooling air mass flow rate, kg/s
P = pressure, Pa
P_F = cooling fan power consumption, W
P_I = motor input power, W
Pr_t = turbulence Prandtl number
Q_C^A = armature cap region copper loss, W
Q_{coil}^F = copper loss in field stack, W
Q_{Iron} = total iron loss in motor, W
Q_{Iron}^A = iron loss in armature stack, W
Q_{Iron}^F = iron loss in field stack, W
Q_S^A = armature stack region copper loss, W
Q_{stack}^A = armature stack region total loss, W
R = ideal gas constant
R = electrical resistance of copper coils, Ω
R_A = radius of the armature stack, m
R_C = cap region coil resistance, Ω
R_{coil}^F = field coil electrical resistance, Ω
R_S = electrical resistance of copper wire in the armature stack region, Ω
$\mathbf{r}$ = location vector
$\bar{S}$ = mean rate of strain tensor
S_A = total heat loss in armature, W
S_{total} = total motor heat generation, W
T = temperature, °C
$\bar{T}_A$ = average armature temperature, °C
$\bar{T}_{\text{air}}$ = average cooling air temperature, °C
T_0 = surrounding air temperature, °C
t = time, s
$\mathbf{U}$ = velocity vector
U_{av} = area averaged velocity, m/s
Γ = total velocity gradient, 1/s
Γ_A = axial velocity gradient, 1/s
Γ_τ = circumferential velocity gradient, 1/s
ε = rate of turbulence dissipation
η = motor efficiency
κ = turbulence kinetic energy
μ = viscosity
μ_t = turbulence viscosity
μ_0 = molecular viscosity
ρ = air density, kg/m^3
ρ_S = solid density, kg/m^3
$\bar{\tau}_{\text{eff}}$ = effective stress tensor
τ_q = external shaft torque
Φ_A = armature diameter, m
$\boldsymbol{\Omega}$ = rotation vector
ω = shaft rotation speed, kRPM

Introduction

UNIVERSAL electric motors are popularly used in industry devices and home appliances due to their simplicity, reliability, and low cost. A universal motor consists of a field assembly, an armature assembly, two carbon brushes, a cooling fan, and one or two brackets that hold the shaft supporting bearings (Fig. 1a). The field lamination stack and the pair of field coils together (Fig. 1b) provide a magnetic field for the armature. In this configuration, the direction of the magnetic field and the orientation of the armature coil wire in the stack slots (Fig. 1c) are perpendicular to each other. With such a relative orientation between the magnetic field and the electrical current, a force is generated on the armature coil when the motor is energized. The overall effect of this electrical–magnetic force is a torque on the armature shaft. As the armature turns, the commutator and two carbon brushes maintain the direction of the torque by switching the direction of the electrical current in the armature coils. In addition, the direction of the torque does not depend on the direction of the external electrical current due to the following two facts: 1) the magnetic field in the motor is generated by the external current, and 2) the external electrical current passes through the field coils and the armature coils in a sequential fashion. With such adaptability on the power source, the application areas of universal motors are significantly increased.

When the electrical current passes through the armature and field coils, heat is generated. This part of the heat generation is called I^2R loss or copper loss. In the field lamination stack and the armature lamination stack, the magnetic field and its variation with time also generate heat, which is called eddy current loss or iron loss. In addition, the friction in the bearing, the friction between the brush and commutator, and the friction of the air also generate heat. All the heat generated has to be dissipated to maintain the motor below a safe

Received 4 February 2009; revision received 7 October 2009; accepted for publication 26 October 2009.

*Senior Project Engineer, 2201 Dwyer Avenue; HL3@uakron.edu.

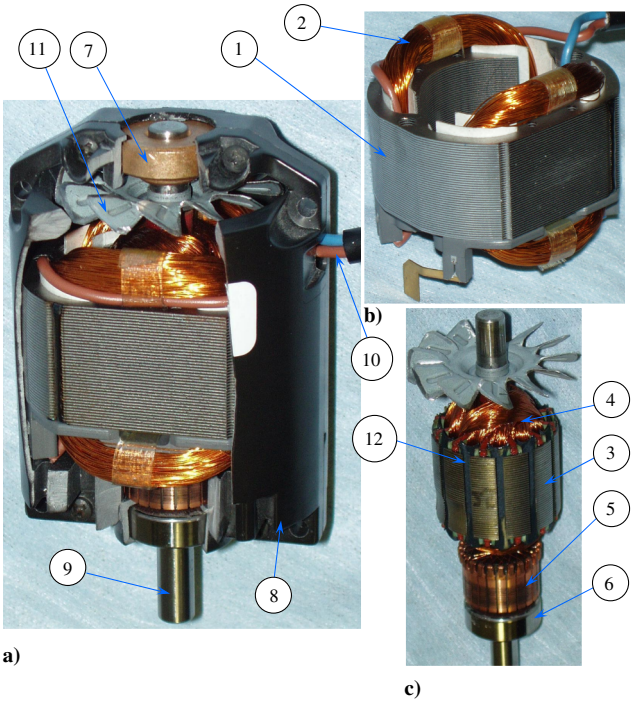

Fig. 1 Universal electric motor with a stamped metal cooling fan: a) motor unit, b) field assembly, and c) rotor assembly. 1, field stack. 2, field coil. 3, armature stack. 4, armature coil. 5, commutator. 6, commutator-end bearing. 7, cooling fan end bearing. 8, motor brackets. 9, shaft. 10, power lead. 11, stamped metal cooling fan. 12, wire slots in the armature stack.

temperature limit. In other words, a cooling system has to be employed in a universal motor designed to run continuously.

Cooling is a critical issue in the electric motor design and manufacturing industry. A good cooling design can improve not only the motor efficiency but also the motor operational reliability [1–3]. A well-designed cooling flowpath can significantly reduce the motor noise level, which has become a critical concern in the current home appliance market [4–6]. In addition, the life of an electric motor depends on the armature and commutator temperatures, which are determined by the motor cooling design [7]. Engineers have realized that the design of electric machines should not focus on the electrical design only. Instead, the good command and control of all different disciplines of electrodynamics, thermodynamics, metallurgy, chemistry, static and dynamic strength of structures, and kinetics is necessary [8]. To date, the majority of electric motors are cooled by air [9–19]. The efforts found in the literature on motor air cooling are summarized in the following paragraphs.

Lee et al. [9] developed a general technique for the thermal analysis of an open-type induction motor with forced cooling channels in the rotor and in the stator. A thermal network method was used in which the coolant network and noncoolant network were coupled together and solved interactively. The coolant was from an external source instead of being driven by a cooling fan built in the motor. Nonaka et al. [10] studied the ventilation and cooling of an induction motor. An analytical method was developed to provide relatively precise results in a short period of time by simple calculation. In this method, the ventilation system and the cooling system were separated. The former was solved by a fluid network using experimental formulas, whereas the later was solved by a quasi-three-dimensional steady-state finite element analysis. Hay et al. [11] presented various formulas (correlations between Nusselt number and Reynolds number) for the convention heat transfer on various regions in an induction motor. These formulas were used in the cooling network thermal analysis of the motor. All the theoretical efforts were based on the fundamental heat transfer equations, which presented the overall cooling of the motor. However, the cooling flow characteristics and local heat transfer on the heat generating components were not explained.

Szogyen [7] emphasized a system design methodology. The motor cooling design should be integrated into the motor design process, instead of being simplified down to a cooling fan selection at the end. Bone's [8] experiences showed that the thermal consideration was the major limitation to the output obtainable from electric machines. However, in reality, the cooling circuits of electric motors never got the attention that was normally directed to electrical and magnetic circuits. Other than the output rate, the life of electric motors was limited by the insulation materials used. The rate at which the insulation materials "age" was approximately doubled for each additional 10°C temperature rise. Sapojnikoff [12] summarized his experience on the selection and installation of cooling fans. The following were the tips on getting the most cooling from the right cooling fans:

1) Avoid mounting obstructing surfaces close to the fan or close to the exit port.

2) Consider using two small fans instead of one large fan.

3) Identify the heat generating elements and concentrate them near the exit port.

4) Reduce the flow resistance of air filters.

5) Smooth out the rough edges.

6) Intensify the cooling on the hot spots by using deflective vanes.

Other than the theoretical work and the summaries of design experience, investigations were also carried out on specific cooling designs, cooling fan optimization, and heat transfer enhancement. Khoze et al. [13] studied the flow organization for two-phase streams and the heat and mass transport process for air evaporative cooling of an electric actuating motor. One desirable structural arrangement was described and experimentally tested. Experimental data were correlated to obtain heat transfer formulas. In this experimental work, it was found that the heat generation in the rotor was substantially nonuniform over its length. Burmester [14] analyzed the air cooling in a square frame dc motor at a high output power level. He reported that the continuous torque ratings of electric machines were largely determined by the cooling intensity. Separated ventilation could increase the motor power rating. The preferred cooling flow design was one in which the cooling fan pushes the air through the motor instead of sucking the air out of the motor. The commutator should be at the upstream of the motor cooling flow. The optimized cooling design increased the motor torque rating by 12%. Woodard and Johnson [1] reported that the heat flux on the rotor surfaces was intensified by the rotor rotation in an axial cooling flow, although the effect and mechanism of such intensification were not explained. The research work by Nakahama et al. [3] on the axial cooling fan design showed that an optimization of the fan parameter, such as blade angles and the blade inclination, increased the cooling airflow rate by 80%. Sheu [15] developed a preliminary numerical procedure for the optimization of axial flow cooling fan design, based on the fundamental fluid flow equations. Nakahama et al. [16] analyzed the cooling airflow in an open-type induction motor. The flow separation on the cooled surfaces was visualized. They also reported that the flowpaths on both sides of the stator cooling core contribute to the cooling performance.

Dessouky et al. [17] investigated a new stator lamination, with which a finned surface was formed on the stator. Farsane et al. [18] experimentally studied an optimized cooling design that resulted in a 10°C reduction on the motor temperature. Chen et al. [19] studied the cooling of an induction motor focusing on the heat transfer enhancement fins and fin parameter optimization. All the heat transfer enhancement efforts were on the stator surface. To date, there is no cooling enhancement technique on the rotor/armature surface reported.

Most of the published studies found in the literature are experimental work or summaries of design and manufacturing experiences. Such studies only provided the overall effects of the cooling air but not the detailed flow structures, temperature distributions, and local cooling densities. Investigations into the performance of stamped metal cooling fans in universal motors have not been found in the literature. In the manufacturing industry, the cooling design of universal motors still relies on trial and error based on experience. The lack of understanding of the local heat transfer and cooling

mechanism prevents engineers from design improvements and system optimizations. A detailed flow driving process of the cooling fan and the flow structures in the motors will help engineers with the motor cooling design and system optimization.

Scope of Work

In this paper, the air cooling of a universal electric motor equipped with a stamped metal axial flow cooling fan will be studied experimentally and numerically. The structures of the cooling flow along the flowpath will be presented. The fluid driving process of the cooling fan, the convection heat transfer on the armature surfaces, and the temperature distribution in the armature lamination stack will be analyzed.

Flow Testing System

Figure 2 shows the experimental flow testing system, which consists of a test section, an air supply unit, and a power supply unit. The universal motor being tested is installed on the top of an air tank. The cooling fan of the motor sucks air from the air tank through the motor and pushes the air into the surrounding environment. The air supply to the air tank is from a compensating air blower unit. The pressure and temperature of air in the tank are measured and monitored.

The regulated power supply, a model 5001i 5kVA power source manufactured by California Instruments, provides the universal motor with ac power at a constant voltage. The outputs of the regulated power source are measured by the power analyzer, a model 5100 single-phase power analyzer manufactured by Magtrol. The uncertainties of the power analyzer readings are 0.01 V, 0.001 A, and 0.01 W for the voltage, current, and power, respectively. The output voltage of the regulated power source can be adjusted with an increment of 0.01 V. A strobe light, a model 1546 electronic stroboscope manufactured by IET Labs, Inc., which is not shown in Fig. 2, is used to measure the motor rotation speed. The stroboscope has a flash duration of 1.2 μs and the uncertainty in frequency measurement is 0.01%. The rotation speed of the universal motor is adjusted with the output voltage of the regulated power supply based on the stroboscope reading.

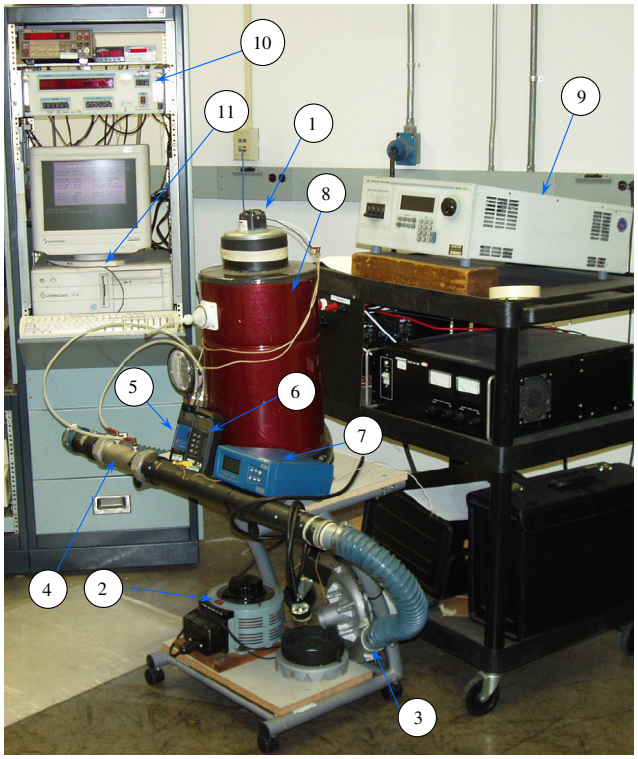

Fig. 2 Experimental flow testing system. 1, the universal motor. 2, autotransformer. 3, air supply blower. 4, flow meter. 5, digital monometer. 6, digital thermocouple reader. 7, air tank pressure indicator. 8, air tank. 9, regulated power supply. 10, power analyzer. 11, data processing computer.

The compensating air blower, an Ametek motor-fan unit model 121031-00, pumps air into the air tank. The unit that supplies power to the compensating air blower is a type 2PF136 PowerStat autotransformer, manufactured by Superior Electric. The output voltage of the autotransformer controls the speed of the compensating air blower motor, which in turn determines the air supply rate. The autotransformer is adjusted to achieve the specific pressures in the air tank.

A flow meter in the pipeline between the compensating blower and the air tank measures the airflow rate supplied into the air tank, which is also the flow rate of the cooling air through the universal motor. The flow meter is a model 50MW20-2 pressure-drop-type flow meter manufactured by Meriam Instrument. A digital monometer reads the pressure drop across the flow meter and the flow rate is calculated according to a calibrated flow rate–pressure drop curve. The obtained flow rate data have an uncertainty of 1%. The temperature in the air tank is measured by a K-type thermal couple and an Omega HH11 digital thermal couple reader. The thermal couple is installed right below the rubber booth on which the electric motor sits. The uncertainty in temperature measurement is ± 0.2°C. The pressure in the air tank is measured by a Druck DPI 150 pressure indicator, a product of General Electric. The purpose of the temperature measurement is to supply an accurate temperature boundary condition for the numerical model.

The pressure measurement location is at the upper half of the air tank. One should note that the volume of the air tank is relatively large and the air velocity is very low. The measured pressure is essentially the total pressure of the air. The purpose of the pressure measurement is to make sure that the gauge pressure of the air flowing into the motor is zero. This is to mimic the actual working condition of electric motors. In actual applications, the motor cooling fan sucks air from its surrounding environment and pushes the air into the surrounding environment again. In other words, the inlet flow and outlet flow are both at the surrounding pressure. Because of this reason, the correlation between the cooling flow rates and the cooling fan rotation speeds is obtained in the following manner. First, adjust the output voltage of the regulated power supply to achieve a certain motor rotation speed. Second, adjust the autotransformer to establish a zero gauge air pressure in the air tank. At this time, the rotation speed is accurately measured by the stroboscope. The rotation speed and the cooling airflow rate, one data pair, are recorded by the data acquisition computer. By increasing the output of the regulated power supply by 5 V and repeating this operation, a set of data pairs is then obtained. These data pairs will show the correlation between the cooling flow rates and the motor rotation speeds.

Numerical Model

The flow of the cooling air is simulated numerically. A schematic of the three-dimensional numerical domain is shown in Fig. 3. The coordinate system is chosen such that the z axis is aligned with the centerline of the motor shaft. The origin of the coordinate system is at the center of the armature stack. The numerical domain is constructed according to the actual design parameters of the universal motor unit, including the dimensions of the cooling fan, the bracket, the armature, the field lamination stack, and field coils. Without listing all of them, only the ones that are critical to the motor performance or critical to flow of the cooling air are given next.

The diameter of the cooling fan is 45.7 mm (1.8 in.). The cooling fan blade thickness is 0.635 mm (0.025 in.) with all the edges sharpened (see Fig. 1). The blade length is 10.2 mm (0.4 in.) and the blade angle is 37.2 deg. The diameter of the armature stack is 34.9 mm (1.375 in.). The height of the armature stack and the field stack is 25.4 mm (1 in.). The diameter of the commutator is 19.1 mm (0.75 in.). The shaft diameter is 8.0 mm (0.315 in.). The laminations in the field and armature stacks are all 0.51 mm (0.02 in.) in thickness.

To simplify the numerical representation of the physical motor, the following simplifications and assumptions are made.

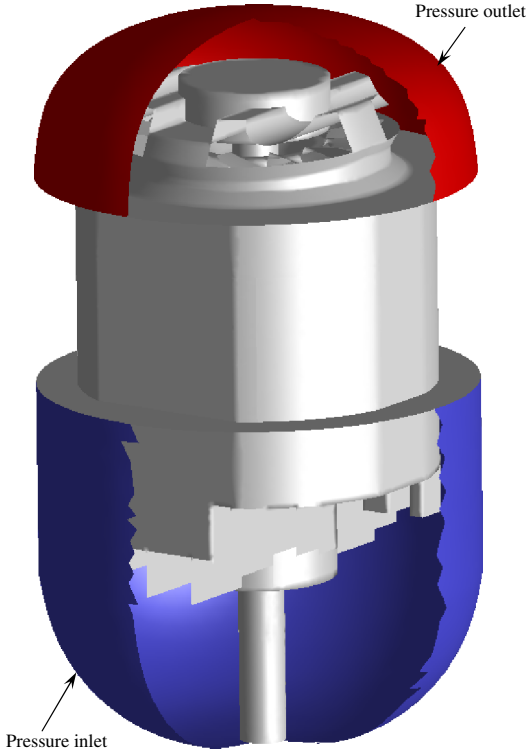

Fig. 3 Three-dimensional numerical model embodiment.

1) The field lamination stack is simplified into a solid body with the heat conductivity in the z direction different from the heat conductivity in the x and y directions. The lower heat conductivity in the z direction represents the overall effects of the conduction heat transfer resistance associated with the interface between the lamination layers.

2) The thickness of the electrical insulation paper between the field coil and the field stack is not considered.

3) The thickness of the cooling fan blades (0.635 mm, 0.025 in.) is neglected (Fig. 3). The blades are represented by three-dimensional surfaces, of which both sides are set to be nonslipping rotating walls.

4) On the flow outlet surfaces of the numerical domain, a uniform pressure condition is assumed.

5) On the flow inlet surface, a uniform pressure is specified.

6) The lamination stack of the armature is modeled as a solid body with different heat conduction coefficients in the axial and radial directions to consider the layer structure (same as for the field stack).

7) Small structures on the lamination punching, such as the copper wire slots, are not considered. The thermophysical properties of the lamination steel are used for both the field and armature stacks.

8) The two cap sections of the armature are assumed to be solid regions and properties of copper varnish mixture are used in the model.

9) All the surfaces of the motor brackets are assumed adiabatic, due to the low heat conductivity of the bulk molding compound material.

10) All the solid surfaces of the cooling fan, the lamination stacks, and the brackets are assumed hydraulically smooth.

11) The majority of the armature stack surface is embraced by the field lamination stack. The difference between the temperature on the armature surface and the temperature on the field lamination is small. The cooling of the armature is mainly by the convection of the cooling air. Radiation heat transfer is not considered.

12) The effects of the friction between the carbon brush and the commutator and the friction in the shaft support bearings are neglected. All the heat generations in the motor are the results of electrical and magnetic energy losses.

For both the inlet flow and the outlet flow, the space of fluid outside the motor is added into the numerical domain. On the spherical surface of the added regions, the surrounding pressure (zero gauge pressure) is specified. Such regions are used in the numerical domain to avoid specifying boundary conditions on the bracket opening slots. At the opening slots of the brackets, the pressure and flow velocities are all unknown and nonuniform. A simplified boundary condition set, uniform velocity or uniform static pressure, will lead to unrealistic flow and pressure fields in the motor. The effects of such unrealistic boundary conditions will be discussed later in this paper.

The mathematical formulation of the numerical model includes the continuity equation, the momentum equation, and the energy equation. In the absolute velocity and vector format, the governing equations in the fluid domain are Eqs. (1–5):

$$\frac{\partial \rho}{\partial t} + \nabla(\rho \mathbf{U}) = 0 \tag{1}$$

$$\frac{\partial(\rho \mathbf{U})}{\partial t} + \nabla \cdot (\rho \mathbf{U}_r \mathbf{U}) + \boldsymbol{\Omega} \cdot \mathbf{U} = -\nabla P + \nabla(\mu \nabla \mathbf{U}) \tag{2}$$

$$\frac{\partial(\rho E)}{\partial t} + \nabla(\rho \mathbf{U} \cdot (\rho E + P)) = \nabla(k_{\text{eff}} \nabla T + \bar{\bar{\tau}}_{\text{eff}} \cdot \mathbf{U}) \tag{3}$$

The air pressure, density, and temperature are governed by the ideal gas law $P/\rho = \mathrm{R}T$, where R is the ideal gas constant. $\boldsymbol{\Omega}$ is the rotation vector of the cooling fan. $\mathbf{U}_r$ is a vector defined by $\mathbf{U}_r = \mathbf{U} - \boldsymbol{\Omega} \cdot \mathbf{r}$. $\mathbf{r}$ is the location vector. k_{eff} and $\bar{\bar{\tau}}_{\text{eff}}$ are the effective thermal conductivity and stress tensor, respectively. The effective fluid thermal conductivity includes molecular conductivity and the turbulence thermal conductivity, $k_{\text{eff}} = k + C_p \mu_t / Pr_t$. The total viscosity, μ, in Eq. (2) is the sum of the molecular viscosity, μ_0, and turbulence viscosity, μ_t. The turbulence viscosity, used in the calculation of effective thermal conductivity and the total fluid viscosity, is obtained by $\mu_t = \rho C_\mu \kappa^2 / \varepsilon$ with an empirical constant $C_\mu = 0.09$. The turbulence kinetic energy, κ, and dissipation rate, ε, are governed by the standard κ–ε transport equations.

$$\frac{\partial}{\partial t}(\rho k) + \nabla(\rho k \mathbf{U}) = \nabla \cdot \left[\left(\mu + \frac{\rho C_\mu k^2}{\varepsilon \sigma_\varepsilon} \right) \cdot \nabla k \right] + G_k + G_b - \rho \varepsilon - Y_M \tag{4}$$

$$\frac{\partial}{\partial t}(\rho \varepsilon) + \nabla(\rho \varepsilon \mathbf{U}) = \nabla \cdot \left[\left(\mu + \frac{\rho C_\mu k^2}{\varepsilon \sigma_\varepsilon} \right) \cdot \nabla \varepsilon \right] + C_{1\varepsilon} \frac{\varepsilon}{k} (G_k + C_{3\varepsilon} G_b) - C_{2\varepsilon} \rho \frac{\varepsilon^2}{k} \tag{5}$$

The air density fluctuation contributes to the overall turbulence dissipation rate, $Y_M = 2\rho\varepsilon k / a_s^2$, where a_s is the speed of the sound. The generation of turbulence kinetic energy, $G_k = 2\mu_t \bar{\bar{S}} \cdot \bar{\bar{S}}$. The generation of turbulence due to buoyancy force (temperature variation), $G_b = -\mathbf{g} \mu_t \nabla \rho / (\rho Pr_t)$. $\bar{\bar{S}}$ is the mean rate of the strain tensor in the fluid and $\mathbf{g}$ is the gravitation vector. The empirical constants, in Eqs. (4) and (5), are $C_{1\varepsilon} = 1.44$, $C_{2\varepsilon} = 1.92$, $\sigma_k = 1.0$, and $\sigma_\varepsilon = 1.3$. $C_{3\varepsilon}$ is calculated by Eq. (6), where U_x, U_y, and U_z are the air velocity components in the x, y, and z directions, respectively.

$$C_{3\varepsilon} = \tanh(|U_z| / \sqrt{U_x^2 + U_y^2}) \tag{6}$$

$$\frac{\partial}{\partial t}(\rho_S h_S) + \nabla(\boldsymbol{\Omega} \cdot \mathbf{r} \cdot \rho h_S) = \nabla \cdot (K_S \nabla T) + S_S \tag{7}$$

The governing equation of heat conduction in the solid regions, in vector format, is given in Eq. (7). The solid enthalpy, h_S, is defined by

$$h_S = \int_{T_{\text{ref}}}^{T} C_p \, \mathrm{d}T$$

Table 1 Solid material properties used in the numerical model

Regions	Density ρ, kg/m^3	Heat capacity C_p, J/kg/K	Conductivity K, W/m/K
Stack regions	8440	377	$K_z = 1.12$, $K_x = K_y = 44.2$
Armature cap region	5947	718	238
Motor shaft	8038	502.5	16.3

Table 2 Results of the grid independence study; $\omega = 10.25$ kRPM; $\tau_q = 5.65 \times 10^{-4}$ Nm (8 oz · in.)

Grids	1	2	3
Size, k	1157	1810	2640
Cooling flow rate, g/s	$M_1 = 1.986$	$M_2 = 2.043$	$M_3 = 2.054$
Difference $(M_i - M_{i-1})/M_i$	——	2.84%	0.55%

where the subscript S is a general representation of solid regions. In different solid regions, different material properties are used; see Table 1. In the rotating armature, $\mathbf{\Omega}$ is the armature rotation vector. S_S is the heat source in the solid, including the iron loss and the copper loss. In the stationary solid regions, the field stack, the rotation speed is zero and the second term on the left-hand side of Eq. (7) becomes zero.

The numerical solution of the above partial differential equation set employs a finite volume discretization approach. The three-dimensional mesh employed is an unstructured tetrahedral mesh with finer cells on the wall surfaces. The relaxation factors for the mass, momentum, energy, turbulence kinetic energy, and turbulence dissipation rate are 0.8, 0.6, 0.9, 0.8, and 0.8, respectively. The iterative solution procedure continues until the residuals of the mass conservation equation, momentum conservation equation, and equations for turbulence quantities are all smaller than 10^{-4}. The residuals of the energy equations are requested to be lower than 10^{-6}. The initial conditions of the first simulation run are zero velocity, zero gauge pressure, and surrounding temperature all across the numerical domain. The later simulation runs employ the results of the previous runs as initial conditions to same computing time. All the simulations were carried on a Dell 690 work station equipped with a 3.0 GHz Intel Xeon dual core processor and a 4 GB memory. One simulation run takes about 16 h until it is fully converged.

To increase the confidence on the results predicted by the numerical models, a grid convergence study is conducted for the case in which the motor runs at 10.25 kRPM (at 8 oz · in. load). The parameters compared include the cooling airflow rate, the armature center temperature, the velocity gradient on the armature surface, and the heat flux on the armature surface. The flow rates of the cooling air through the motor are presented in Table 2. The three flow rates predicted by the three grid densities show a trend that approaches a constant number with the refinement of the grid. In addition, the difference between the results from grids 2 and 3 is negligibly small. The comparison of all the parameters show the same conclusion for the three grid densities. Based on these three facts, the author thinks that grid 3 is fine enough for the numerical simulations of the thermal fluid flow in the motor. All the results presented hereafter are obtained with grid 3.

Results and Discussion

Heat Generation

The rates of heat generation in the armature and field assemblies are calculated from the speed torque test data of the motor. Details on the speed torque testing system, equipments, and testing method can be found in a previous study by the present author [20]. The results of the speed torque test provide the rotation speeds, the motor input power, the output shaft work, and the efficiency of the motor, as shown in Fig. 4. Based on these data, the total heat generation in the motor, S_{total}, can be calculated by $S_{\text{total}} = P_I - \tau_S \cdot \omega$. P_I is the total power input to the motor. τ_S and ω are the measured shaft torque and shaft rotation speed, respectively. The total heat generation in the motor is the sum of the total copper loss and the total iron loss. The total copper loss is the combination of the I^2R losses in the armature coils and the field coils. The total iron loss is the sum of the field stack loss and the armature stack iron loss. In the armature cap region, $Q_C^A = I^2 \cdot R_c^A$. In the armature stack region, $Q_S^A = I^2 \cdot R_S^A$. The copper loss in the field coil is $Q_{\text{coil}}^F = I^2 \cdot R_{\text{coil}}^F$. The copper wire resistances are measured by an Ohm meter. The length of the copper wire in the cap region is length of the copper wire in the armature less the total wire length in the armature stack slots. The total iron loss is then calculated by $Q_{\text{Iron}} = S_{\text{total}} - (Q_C^A + Q_S^A + Q_{\text{coil}}^F)$. The iron loss in the armature and the iron loss in the field stack are calculated based on the magnetic field variation frequency and the total iron loss,

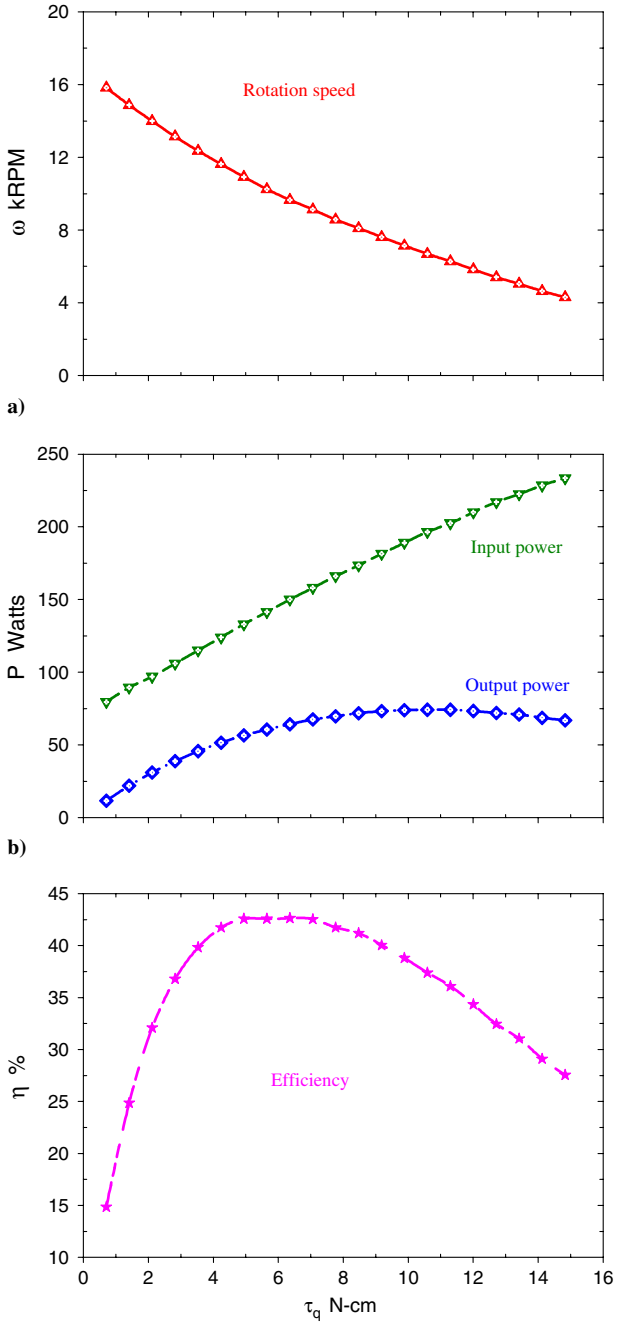

Fig. 4 Performance of the electric motor/results of the speed torque test: a) rotation speeds, b) input power and the output shaft work, and c) motor efficiency.

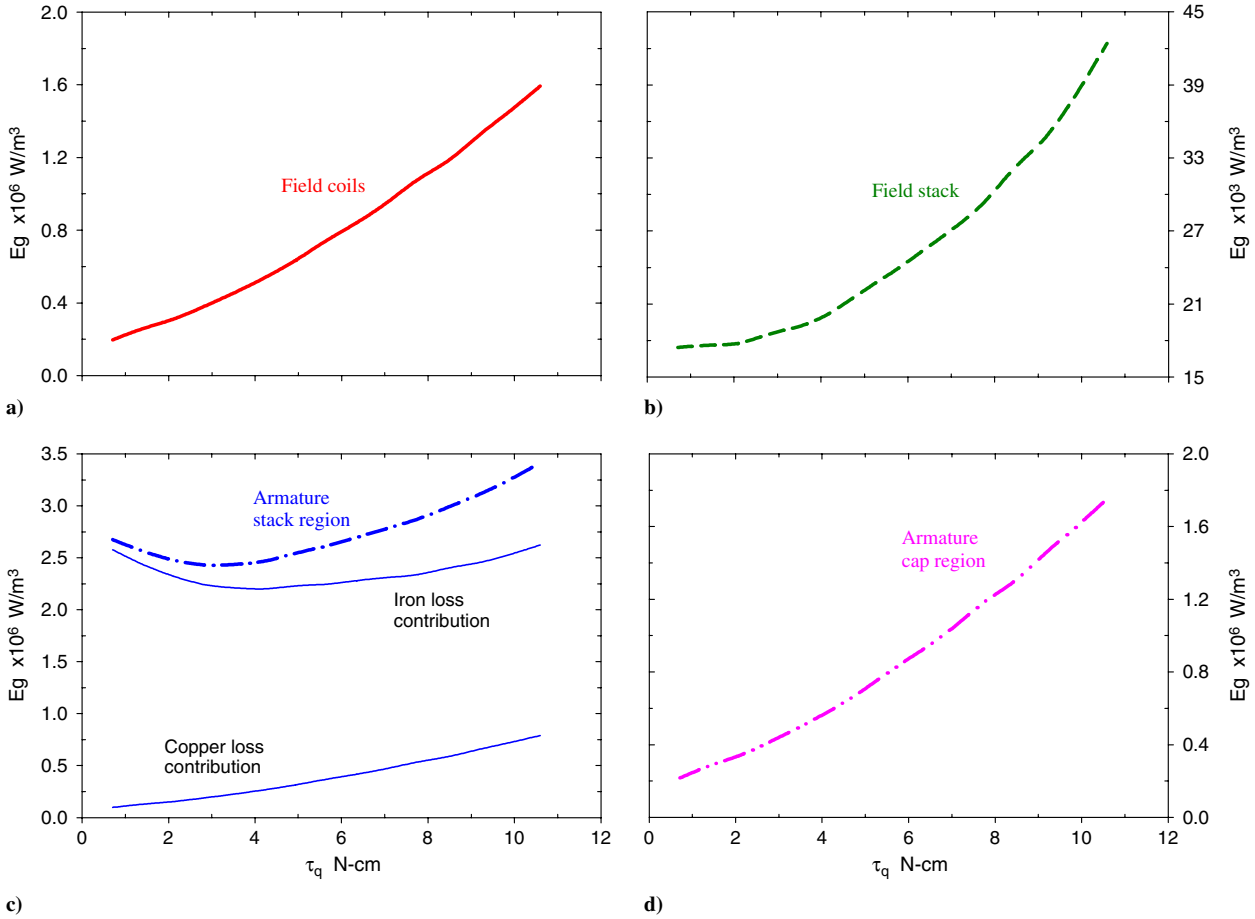

Fig. 5 Heat generation per unit volume in the motor field and armature: a) field coils, b) field stack, c) armature stack region, and d) armature cap region.

$Q_{\text{Iron}} = Q^F_{\text{Iron}} + Q^A_{\text{Iron}}$. Based on these results, the heat generation in the armature stack regions is $Q^A_{\text{stack}} = Q^A_{\text{Iron}} + Q^A_S$. The heat generation in the armature cap regions is Q^A_C. The heat generation in the field coils and the field stack are Q^F_{coil} and Q^F_{Iron}, respectively. For various external loads (shaft torque), the volumetric heat generation rate in the field coils, field stack, armature stack region, and the armature cap regions are given in Figs. 5a–5d. These heat generation data are used to specify the heat source (volume conditions) in the numerical model.

Cooling Flow Rate

The experimentally measured and numerically predicted mass flow rates of the cooling air at various motor rotation speeds are shown in Fig. 6. The agreement is reasonably good. Such a good agreement, together with the grid independence study, validated the numerical model on the following aspects.

1) The simplifications and assumptions made in the physical model of this universal motor are realistic.

2) The mathematical formulation and the corresponding boundary conditions can represent the actual thermal fluid flow process.

3) The grid density is fine enough to catch the detailed structures of the fluid flow and the temperature distributions.

The correlation between the cooling fan rotation speed and the cooling flow rate is close to linear. Such a correlation is due to the actual working condition of the cooling fan. Both the air inlet and the air outlet of the numerical model are at the normal surrounding pressure condition. Along the cooling flowpath, there are no regions with a high gauge pressure or vacuum (high enough to be comparable with the absolute surrounding pressure). In other words, the compressibility of air does not play an important role. The pressure head built by the cooling fan is solely used to overcome the flow resistance in the motor.

Flow Driving of the Cooling Fan Blades

In this section, the fluid driving performance of the cooling fan blades is examined. Figure 7a shows the airflow structure in a z plane (perpendicular to the motor shaft) cutting through the center of the cooling fan. Figure 7b shows the flow structure in a cylindrical surface cutting through the radial center of the blades. Figure 7c shows it in a plane cutting through the circumferential center of one blade, showing the flow of air from the upstream side to the downstream side of the cooling fan.

With the flow structure shown in Fig. 7, one can see that the stamped metal cooling fan drives an axial flow. At the upstream side, the air at the center region is sucked by the cooling fan blades. After the blade region, the flow stream has both a radial component and an axial

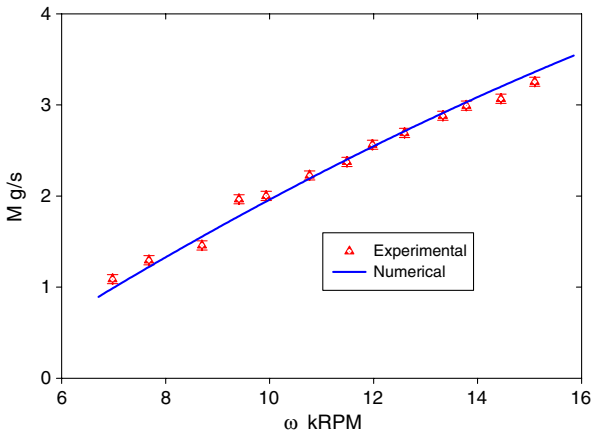

Fig. 6 Mass flow rate of the cooling air at various motor rotation speeds.

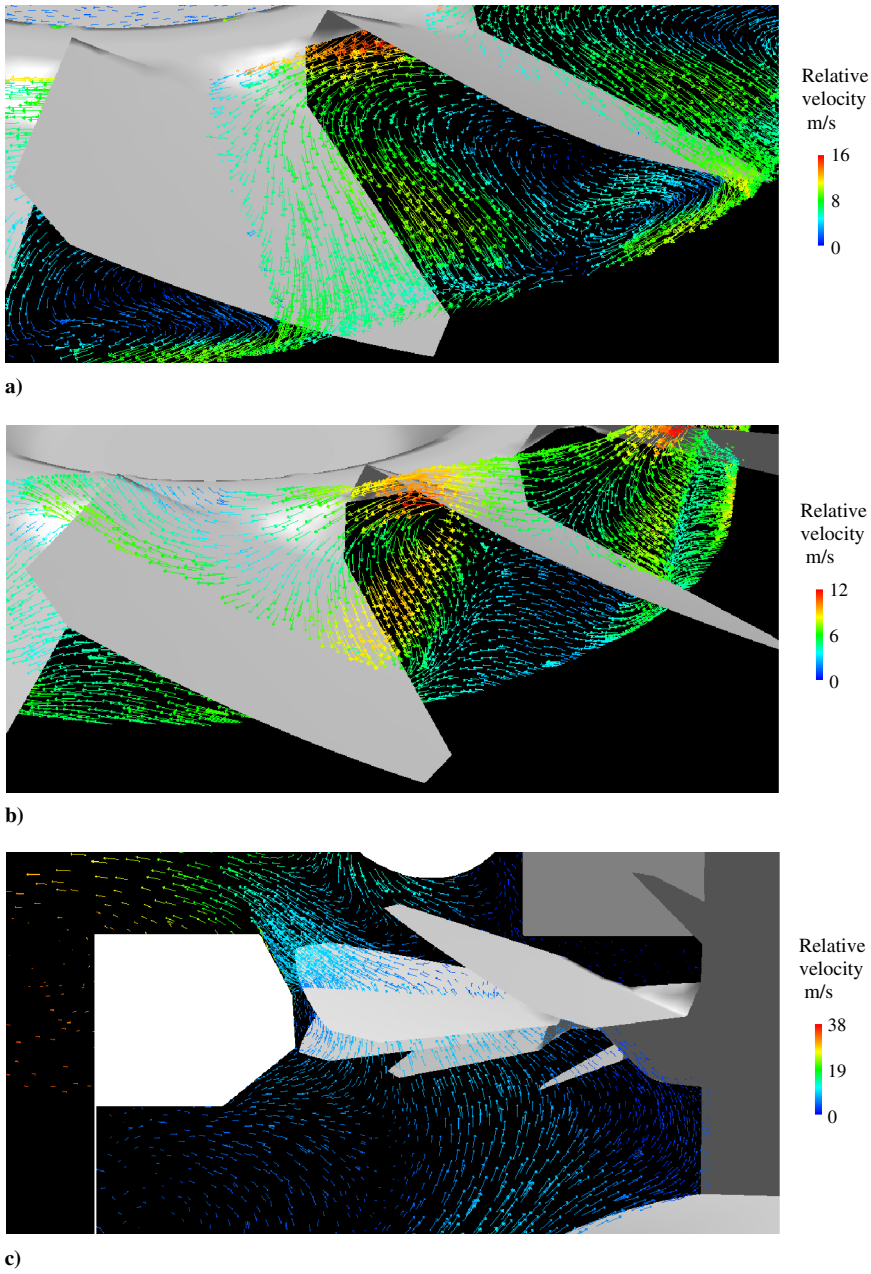

Fig. 7 Airflow structure driven by the stamped metal cooling fan: a) in the z plane cutting the z center of the blades, b) in the cylindrical surface cutting through the R center of the blades, and c) in a radial plane cutting through the θ center of a blade.

component, together with the circumferential component (Fig. 7c). At the downstream side of the cooling fan, the radial component and the axial component are in the same order of magnitude. Comparatively, at the upstream side, the radial component is small. In other words, the stream of the airflow obtains a radial component in the blade region. This can be further seen in Fig. 7b. In the blade region, the airstream follows the orientation of the blade surfaces moving in both the radial and circumferential directions. Figure 7a shows even more clearly the radial movement of the air along the blade surfaces.

There are no flow separations on the cooling fan blades and there are no recirculation cells in the blade region. From the upstream side to the downstream side, the airflow stream has no sharp changes in the flow direction. Both of the aforementioned characteristics of the cooling airflow indicate that the cooling fan blade angle is well chosen for the present motor design.

The power consumption of the cooling fan, nondimensionlized by the power input to the motor, is given in Fig. 8 for various load conditions. As the motor load increases, the cooling fan power consumption decreases, due to the fact that the motor rotation speed is inversely proportional to the external shaft load. At the design working condition, 5.65 N · cm (8 oz · in.), the cooling fan only takes 4.2% of the input electrical power. Even at a high rotation speed (lower load at 6 oz · in.), the cooling fan consumes only 7.1% of the shaft work. These quantified energy consumption data show that the energy consumption of the axial flow stamped metal cooling fan is not significant compared to the motor input power. In the development of motor cooling systems or motor cooling fans, the motor temperature rise and noise level should have a higher priority than the cooling fan energy efficiency.

Flow Structure in the Motor

With the current motor architecture and cooling design, the cooling fan is at the outlet side of the cooling flowpath. The cooling air flows through the motor first before it reaches the cooling fan. After the cooling fan, the air goes into the surrounding environment through the outlet opening slots on the motor brackets.

Along the flowpath, the armature and field assemblies are at the upstream side of the cooling fan. Figures 9a and 9b show the pressure distribution and flow structure in the symmetry center plan of the

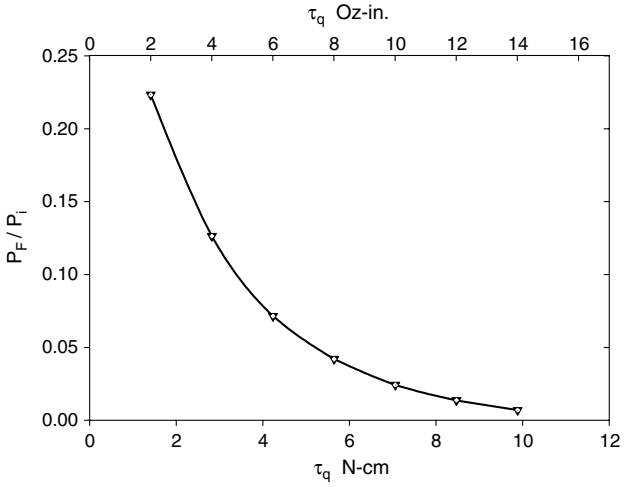

Fig. 8 Power consumption of the cooling fan at various load conditions.

field stack. Sucked by the cooling fan, the cooling air flows out of the motor air slots (between the armature stack and the field stack). This airstream first approaches the center section and then gets sucked into the cooling fan blade region. Different from this flow stream, the flow in the screw holes in the field stack is in the opposite direction. The hot air is brought into the air inlet side of the motor through these screw holes. This flow in the opposite direction is driven by the pressure distribution in the regions at the hole openings. Around the screw-hole opening at the cooling fan side, there is a local high-pressure region. Such a high-pressure region pushes the air back into the screw hole. The distribution of such a high-pressure region is further illustrated in Fig. 9c. In this plane, the pressure at the center is lower and the pressure at the outer region is higher, which is a typical pressure field developed by the rotation of fluids. In Fig. 9d, the flow structure in the same plane proved this point. The velocity of the air shows the air rotation in the same direction as the cooling fan rotation. The magnitude of the rotating air velocity at the outer region in this pane is close to the tip rotation speed of the cooling fan. This flow structure and the quantitative velocity magnitude indicate that the rotation of the cooling fan not only creates the circumferential component of the air velocity at the downstream side of the cooling fan but also develops the air rotation at the upstream side. The induced rotation of the air establishes a high-pressure region. Such a high-pressure region drives the backward leakage through the gaps between the field stack and the motor bracket and through the screw holes. The leakage recirculates the hot air inside the motor. All of the gaps or channels in the outer region should be closed to prevent the recirculation of hot air.

Overall Cooling of the Motor

In this section, the overall cooling of the motor is examined. Figure 10a shows the temperature distribution on the armature surface at the designed working condition. In Fig. 10b, the maximum temperature in the armature body and the volume-averaged temperature in the armature are given for various external load conditions. For the range of external loads studied, the maximum armature temperature is 12–20°C higher than the volume-averaged temperature. The maximum temperature is always on the shaft centerline in the armature stack region. The volume-averaged temperature is a representative of the armature coil temperature. To maintain the motor safely, the armature coil temperature must be kept lower than 150°C for normal universal motor designs that employ varnish to hold the copper coils in place and tightly together. With the volume-averaged temperature under various external loads, one can see that this motor can only run with an external load at 5.65 N · cm (8 oz · in.) or lower. Load higher than 5.65 N · cm will lead to overheating of the armature coils.

The air temperature rises for various external loads are given in Fig. 11a. The air is pulled from its surroundings into the motor. The air inlet temperature does not change with the external loads of

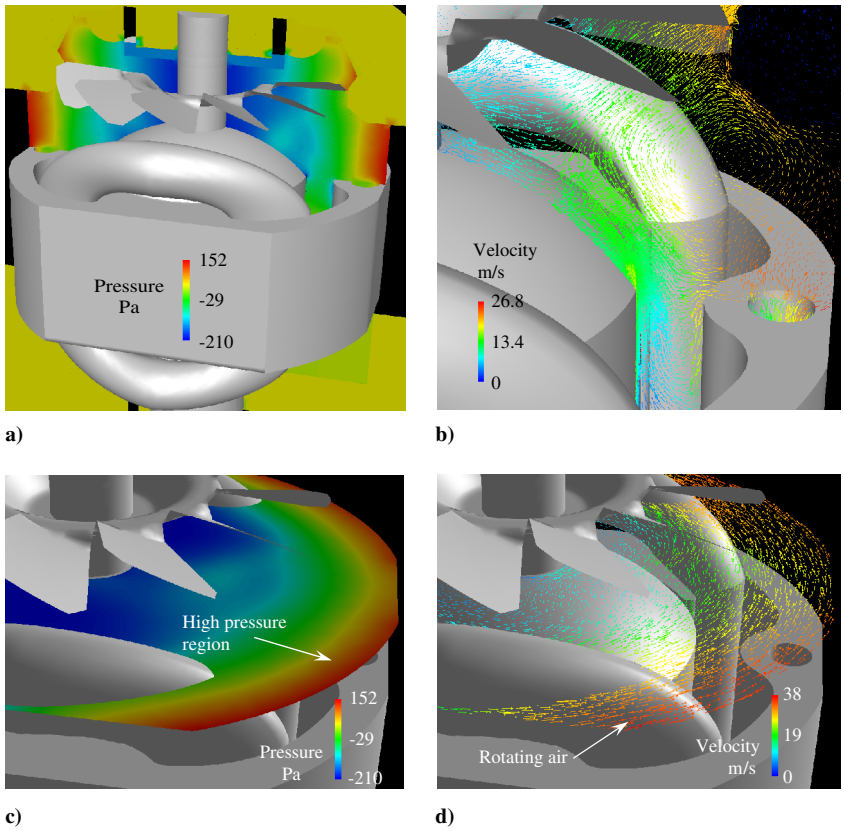

Fig. 9 Effects of the pressure built up by the rotation of the air at the upstream side of the cooling fan: a) pressure distribution in an axial center cross section ($x = 0$ plane), b) flow structure in the $x = 0$ plane, c) pressure distribution in a z plane ($z = 48.4$ mm) perpendicular to the z axis at the upstream of the fan, and d) rotation of the air in the $z = 48.4$ mm plane.

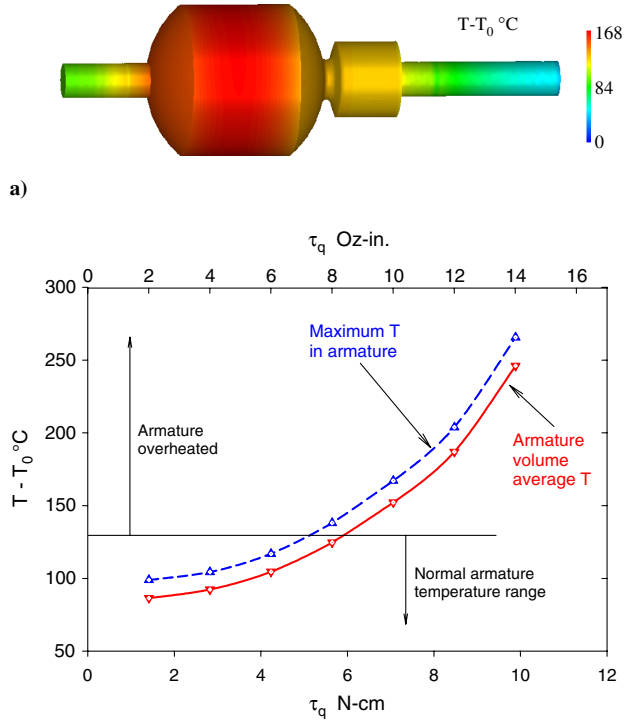

Fig. 10 Armature temperature rise: a) armature and shaft surface temperature distribution at $\tau_q = 0.0706$ Nm (10 oz · in.), and b) maximum and the volume averaged temperature rises in the armature for various external loads.

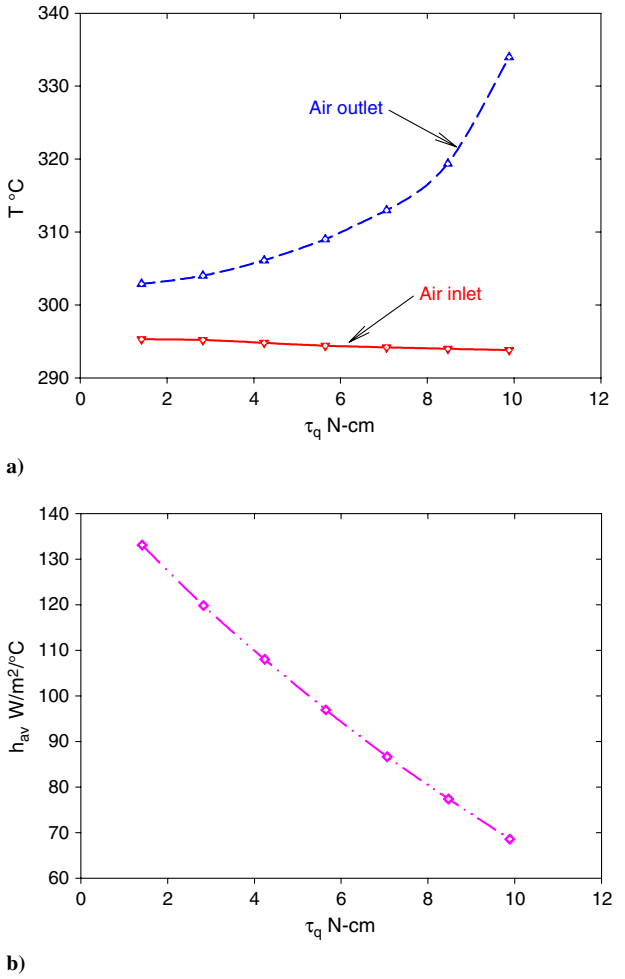

Fig. 11 Overall convection cooling on the armature surface: a) air inlet and outlet temperatures, and b) averaged convection heat transfer coefficient on the armature surface.

the motor. With the increase of the load, the heat generation in the motor increases (Fig. 5). Meanwhile, the flow rate of the cooling air is reduced (Fig. 6). The total effect of these two aspects is that the temperature of the air at the outlet increases quickly as the load increases. With the increased air outlet temperature, the averaged air temperature becomes higher, which also elevates the armature temperature. This can explain what was stated by Burmester [14], that separated ventilation could improve the output rating of electric motors. With separated ventilation, the cooling air is driven by another motor, the speed of which remains constant. With this architecture, as the external load increases, the cooling airflow rate remains the same. Compared to the integrated ventilation, a cooling fan installed on the working motor shaft, motors with separated ventilation have better cooling intensity at high external load conditions.

$$h_{\text{av}} = \frac{S_A}{A_A \cdot (\bar{T}_A - \bar{T}_{\text{air}})} \tag{8}$$

The overall convection heat transfer coefficient on the armature surface is given in Fig. 11b. The definition of the average convection heat transfer coefficient is given in Eq. (8). S_A is the total heat generation in the armature. A_A is the total surface area of the armature. $\bar{T}_A$ and $\bar{T}_{\text{air}}$ are the average armature surface temperature and the average air temperature, respectively. From the previously presented data, one knows that total heat generation, the temperature of the armature, and the temperature of the air all increase with external load. What Fig. 11b indicates is that the increase of the temperature difference between the armature and the cooling air is faster than the increase of the heat generation rate. Such a faster increase of the armature cooling temperature differential is due to the convection on the armature surface. As the external load increases, the lowered cooling airflow rate and the lowered armature rotation speed both contribute to the reduction on the convection heat transfer coefficient.

The temperature on the armature surface at the design working condition is shown in Fig. 12a. Figure 12b gives, quantitatively, the temperature distribution along the centerline of the motor shaft, line A–A. The temperature distribution in the radial direction at the center of the armature stack, line B–B, is given in Fig. 12c. In the axial direction, the temperature variation in armature stack is noticeable. This temperature variation is mainly caused by the low heat conductivity of the stack in the axial direction. Outside the stack section, the temperature variation along the shaft is also large. This large temperature variation indicates a large heat flux along the shaft from the stack region toward the two ends of the shaft. At the locations where bearings are installed, the shaft temperatures are still high. One can conclude qualitatively that the heat flux along the shaft is one of the causes for the high bearing temperature.

In the radial direction, the heat conductivity in the stack region is high. Accordingly, the temperature distributions in the armature stack and in the field stack are both uniform (Fig. 12c). A large temperature variation exists in the air film between the armature and the field stack hood. Such temperature distribution indicates that, when comparing the conduction in the stack and the convection on the armature surface, the convection on the surface carries the main resistance for the cooling heat flow.

Local Cooling on the Armature

The overall convection heat transfer coefficient is determined by the local fluid flow and temperature distributions. In this section, the flow velocity and temperature gradients on the armature surface to understand the convection heat transfer process are examined. On the z center plane of the field stack, the flow structure is shown in Fig. 13a. As explained earlier, there are backward flows in the side slots between the field stack and the motor brackets. In the field stack screw hole, the flow is also backward. In this plane, the flow in the field stack airflow slots also shows sections with backward flows.

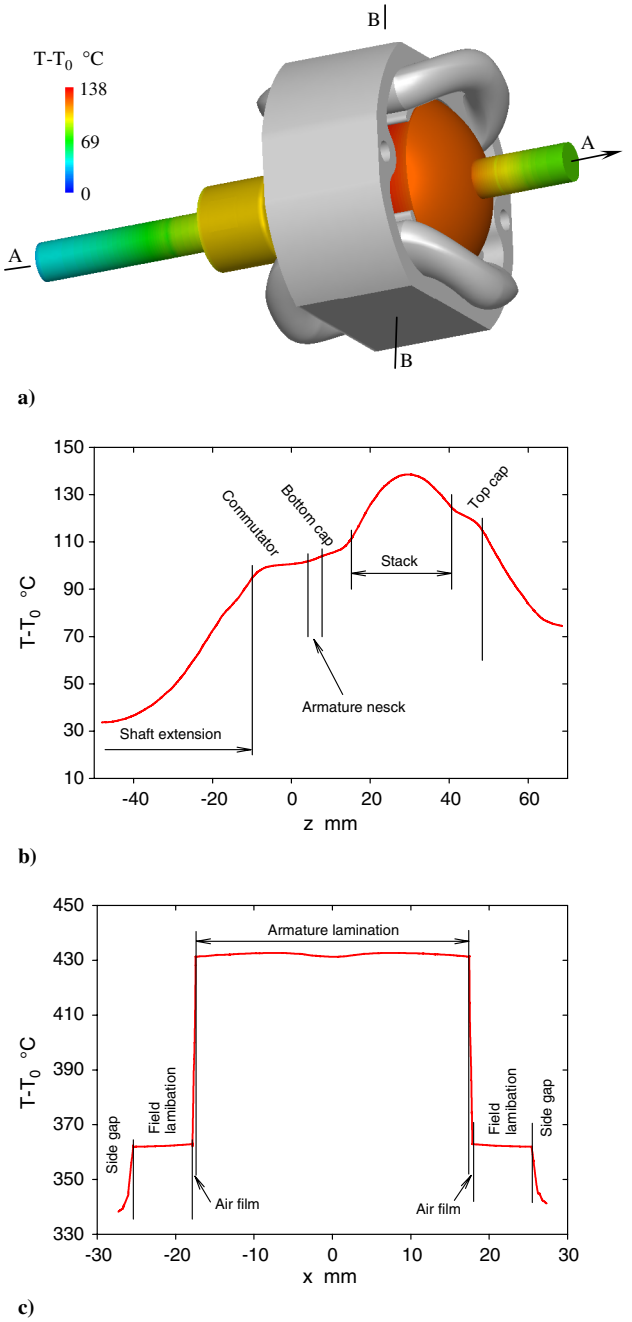

Fig. 12 Temperature distributions inside the armature, $\tau_q = 5.65$ N · cm (8 oz · in.): a) three-dimensional view of the armature temperature map, b) axial distribution along A–A, the centerline of the shaft, and c) radial distribution at the center of the stack along line B–B.

This indicates that the rotation-generated pressure at the upstream side of the cooling fan affects even the flow in the cooling air slots. Another flow phenomenon one should notice is the air films between the armature and the field stack hood. In these air films, the velocity variation/gradient is high.

Figures 13b and 13c give the velocity and temperature distributions cross the air film. One should be reminded that the thickness of the air film is 0.39 mm (0.0155 in.). At this location (the center of the hood region) on the armature surface (along line C–C), the tangential and axial velocity gradients are 1.49×10^5, and 1.26×10^5 1/s, respectively. The total velocity gradient is 1.96×10^5 1/s. The temperature gradient is 5.11×10^5 °C/m. With the current cooling system design, the tangential and axial velocity gradients are at the same order of magnitude at the design working condition. The high temperature gradient indicates a high convection coefficient.

In the air slots, along line D–D, the velocity and temperature distribution are given in Figs. 13d and 13e. At this location (the center of the slot region), the tangential and axial velocity gradients are 1.18×10^5 and 9.92×10^4 1/s, respectively. The total velocity gradient is 1.54×10^5 1/s. The temperature gradient is 1.00×10^6 °C/m. The velocity gradients in the air slots are lower than in the air film. However, the temperature gradient is higher due to the fact that the air temperature in the air slots is lower. The field stack hood temperature is high because of the heat generation in the field laminations and the field coils. Based on these data of the temperature gradient, which is proportional to the local heat flux, one can conclude that the cooling heat flux in the air slots is about two times that in the air film.

$$\Gamma = \sqrt{\Gamma_\tau^2 + \Gamma_A^2} \tag{9}$$

$$\frac{\partial \Gamma}{\partial \Gamma_A} = \frac{\Gamma_A}{\sqrt{\Gamma_\tau^2 + \Gamma_A^2}} \tag{10}$$

On the armature surface, the total velocity gradient is determined by the tangential velocity gradient and the axial velocity gradient, Eq. (9). The tangential velocity gradient is determined by the motor rotation speed. For a given speed, the effect of axial velocity gradient on the total velocity gradient is given in Eq. (10). Considering the variation of the right-hand side of Eq. (9) versus the axial velocity gradient, the ratio between Γ_A and Γ_τ is recommended to be between 0.8 and 1.2. For the current motor design and cooling flow, at the designed working condition, Γ_A/Γ_τ is 0.85 and 0.84 in the hood region and the slot region, respectively. One can see that this velocity gradient ratio is in the lower end of the recommended range. To make the motor work at a higher shaft load, one can increase the airflow rate and make this ratio approach 1.2. One should be reminded about the empirical conclusion stated in Woodard and Johnson [1] that the heat transfer rate on the rotor was intensified by the rotor rotation in an axial cooling flow. The aforementioned quantitative thermal fluid data and the analysis of the effects on the rotation and axial velocity components explained the mechanism behind this qualitative statement.

Cooling on the Commutator

The architecture of the motor studied is not the one suggested by Burmester [14], in which the cooling fan pushes the air through the motor. One should keep in mind that Burmester's recommendation was for large-size low-speed motors in which the rotor vibration and the shaft critical speeds were not concerns. In such motors, the commutator and the cooling fan can be installed at the same side of the motor.

In high-speed universal motors, the cooling of the commutator is critical because it determines the brush wear rate and the commutator copper bar wear rate. The commutator must work under a temperature limit. Beyond this limit, commutation may fail in the following modes: 1) a quick brush worn out, 2) commutator copper bar damage, and 3) serious sparking/arching. Any of these problems can lead to the end of the motor life. To maintain a lower commutation temperature, the commutator in a universal motor is normally installed at the upstream section of the cooling flowpath. The advantage is that the air surrounding the commutator is at a low temperature.

Different from large-size low-speed motors, high-speed universal motors have an armature vibration issue when the motor rotation speed is close to the shaft critical speed. In this situation, the length of the shaft is important because the critical speeds and the length of a shaft are inversely proportional. In designing a small universal motor, the cooling design and the motor vibration have to be considered together. More shaft space is needed when putting the commutator and the cooling fan at the same side of the armature stack. Considering the aforementioned reasons, high-speed universal motors normally have the commutator at the upstream side whereas the cooling fan is installed at the downstream side of the armature

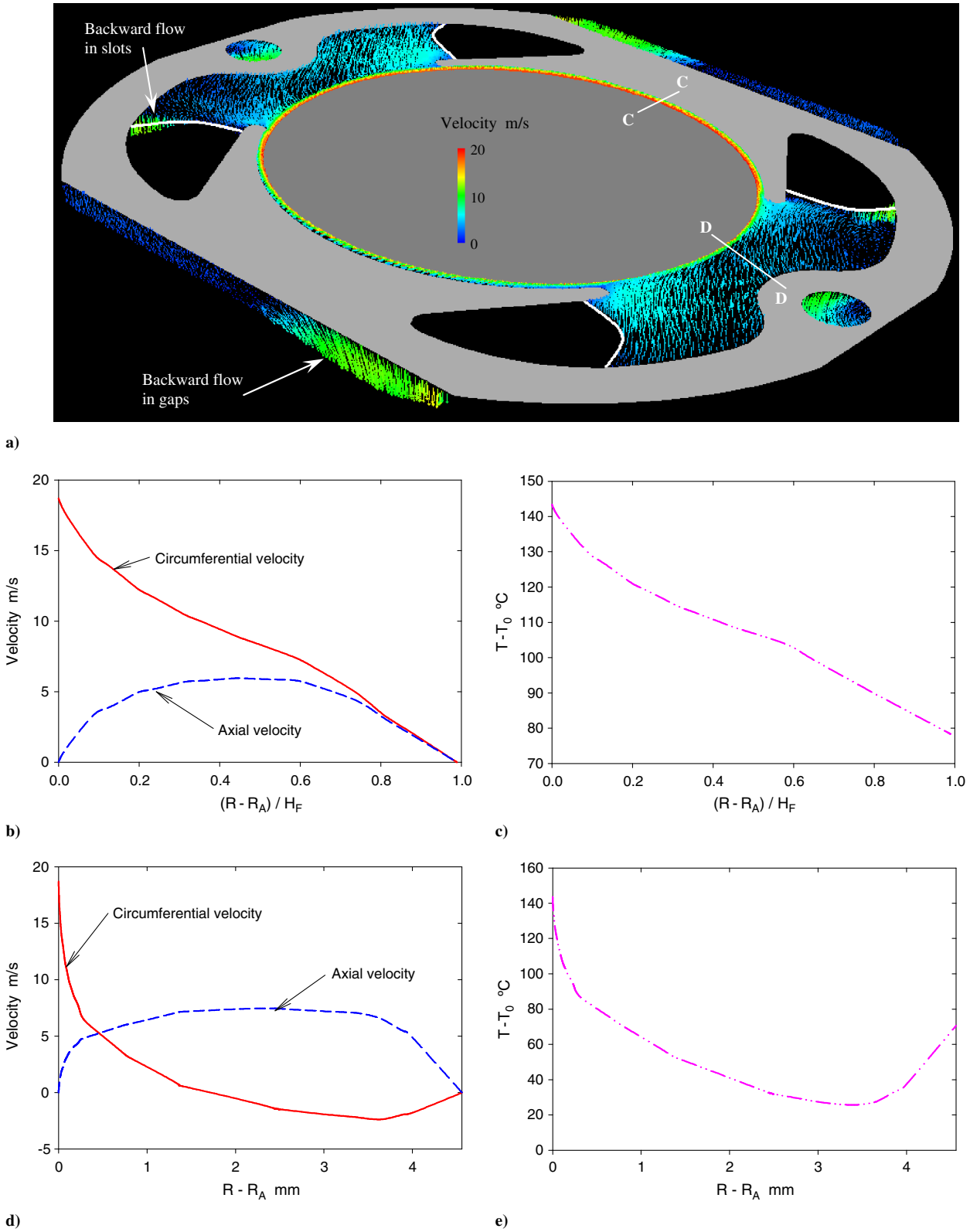

Fig. 13 Flow and temperature at the armature stack surface, $R_A = 17.463$ mm (1.375 in.), $H_F = 0.394$ mm: a) three-dimensional view of the flow at the center of the stack, b) velocity across the air film at C–C, c) temperature across the air film at C–C, d) velocity across the air channel at D–D, and e) temperature across the air channel at D–D.

stack (instead of the architecture suggested by Burmester [14]). With this architecture, the cooling fan pulls the air, instead of pushing the air, through the motor.

In the current design, the fluid flow and temperature around the commutator are given in Fig. 14. One can see that a wall layer flow is developed around the commutator. A high velocity gradient is established on the armature surface. The temperature map in Fig. 14b shows a high temperature in the commutator body and a low surrounding air temperature. This low air temperature helps the cooling of the commutator.

The temperature in the commutator and the carbon brushes are at the same level. A large temperature gradient is only in the wall layer flow. This temperature distribution indicates that the wall layer flow has the major heat transfer resistance for the cooling of the

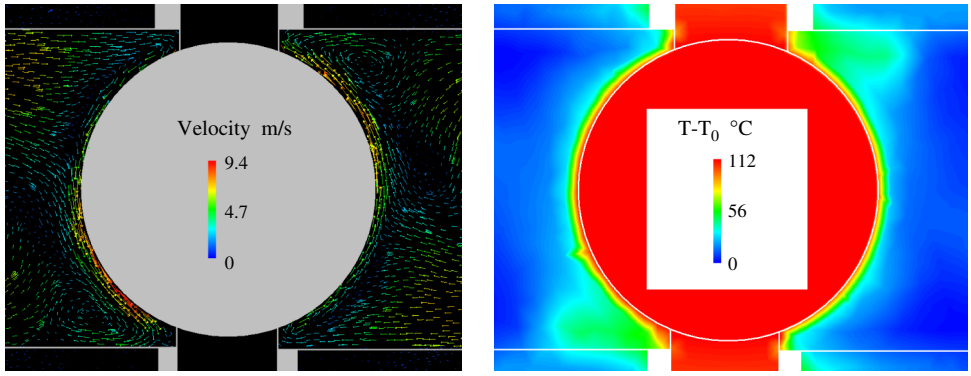

Fig. 14 Cooling of the commutator: a) flow structure around the commutator, and b) temperature on the commutator and carbon brushes. $\tau_q = 5.65$ N · cm (8 oz · in.).

commutator. Commutator cooling enhancement should focus on increasing the convection heat transfer coefficient or increasing the cooling surface area.

Effect of Pressure Boundary Locations

All the results presented earlier were obtained with the inlet and outlet pressure boundaries set on the spherical surfaces, far away from the opening slots on the motor brackets. This boundary is chosen because the boundary locations have significant effects on the cooling flow simulation. In this section, the following two cases are compared. One has the pressure boundaries at the far-field locations (Fig. 15a). The other has the pressure boundaries at the opening slots of the motor bracket (Fig. 15b).

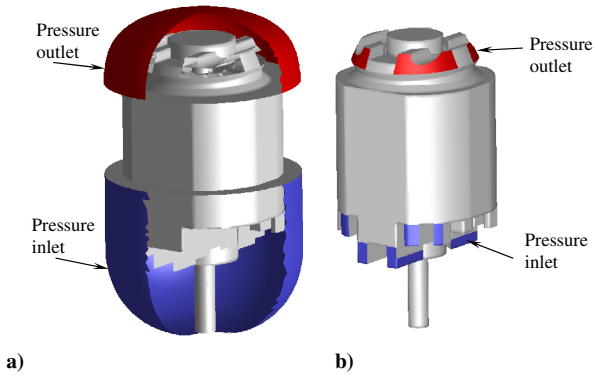

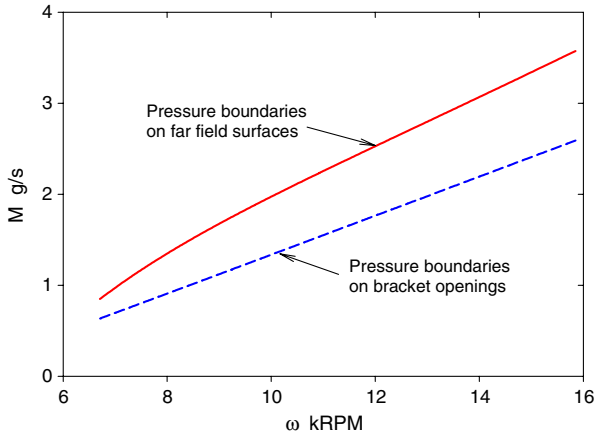

Fig. 15 Effects of the pressure boundary locations: a) pressure boundaries on the far-field surfaces, b) pressure boundaries on the bracket openings, and c) predicted cooling flow rates for the two sets of boundary locations.

Figure 15c gives the cooling airflow rate through the motor for these two pressure-boundary locations. The comparison clearly shows that setting pressure boundary at the bracket opening slots leads to an unrealistic flowfield in the motor. This low flow rate can be explained by the following facts.

1) The actual pressure distributions at the motor bracket opening slots are not uniform. The pressure variations on the opening slots are not negligible compared to the total pressure drop of the cooling flow through the motor. Assuming a uniform pressure (neglecting the pressure variation at the slot openings) leads to an unrealistic flowfield.

2) At the outlet slots of the motor bracket, the air has a high rotating velocity component. As this rotating component reduces, part of the velocity head is recovered into the pressure head in the region outside of the motor brackets. This amount of energy recovery is not negligible because the total pressure drop of the cooling flow through the motor is small.

Remarks on Application

With the magnetic design of the current motor, the motor efficiency is high when the external load is between 4.24 N · cm (6 oz · in.) and 8.47 N · cm (12 oz · in.). The current cooling design can maintain the motor constantly at a safe temperature only when the external load is 5.65 N · cm (8 oz · in.) or lower. Loads higher than 5.65 N · cm will lead to the armature overheating and motor failure. Increasing the flow rate of the cooling air can improve the torque rating of the motor.

The stamped metal cooling fan has the correct blade angle for the current motor cooling design. There is no flow separation and recirculation on the fan blade surfaces. Increasing the cooling flow rate can be achieved by increasing the cooling fan diameter while keeping the blade angle.

The airflow in the gap between the motor brackets and the field stack and flow in the field stack screw holes is backward. Eliminating these backward flows can improve the cooling of the motor.

The heat conduction along the shaft is not negligible. The shaft heat conduction is one of the factors that maintain the shaft supporting bearings at a high temperature. Reducing the heat flow rate along the shaft toward the bearings will lower the bearing temperature.

When the commutator is at the cooling flow inlet side of the motor, the air surrounding the commutator is at low temperature. This low-temperature air helps to keep the commutator temperature rise low. Considering the air temperature rise through the motor, a universal motor architecture with the commutator at the cooling air inlet side is recommended.

Conclusions

The cooling of a universal drive motor with a stamped metal axial flow cooling fan is numerically and experimentally studied. The

agreement between the experimentally measured and the numerically predicted airflow rate data is reasonably good.

In electric motors, the cooling fan overcomes the flow resistance along the flowpath and maintains the cooling flow rate. The pressure head build up by the cooling fan is small. Under this circumstance, the cooling flow rate is proportional to the cooling fan rotation speed. On the electrical side, the armature rotation speed is inversely proportional to the external load. As the shaft load goes up, the heat generation in the armature increases. The increase of the heat generation and the decrease of the cooling flow rate lead to the overheating of the motor when the motor is even slightly overloaded. This explains the fact that cooling is a determining factor for the motor torque rating.

Heat transfer analysis on the armature surface shows that the armature body has a uniform temperature in the radial and circumferential directions, whereas the temperature variation in the axial direction is noticeable. The air velocity gradient on the armature surface is high. This high velocity gradient determines the high convection heat transfer coefficient on both the film region and the slot regions. Because of the high temperature in the air film, the heat flux on the armature in the slot region is higher than in the air film region. At the design working condition, the temperature rise of the air through the motor is large. The increase of the cooling flow rate can reduce the air temperature rise and then the average air temperature. In the meantime, with the motor rotation speed at the design working condition, the circumferential component of the air velocity on the armature surface is not very high. An increase of the cooling flow rate can also increase the axial velocity gradient on the armature surface, which leads to a higher convection heat transfer coefficient.

The rotation of the stamped metal cooling fan not only develops the air rotation at the downstream side of the cooling fan, but also drives the air rotation at the upstream side. The air rotation at the upstream side of the cooling fan leads to the recirculation of the hot air back into the cooling air inlet of the motor. Such hot air recirculation is detrimental to the motor cooling. This flow driving characteristic should be considered when designing the cooling flowpath and the architecture of electric motors. The power consumption of the cooling fan is small compared to the electrical and magnetic energy losses in the motor. The agreement between the flow direction and the cooling fan blade angle indicates that the cooling fan noise generation is not a big concern. The thermal considerations and cooling design improvements should focus on the motor temperature rise.

References

[1] Woodard, J. K., and Johnson, G. E., "Optimal Design of Cooling Fans for Industrial Electric Motors," *Journal of Mechanisms, Transmissions, and Automation in Design*, Vol. 108, No. 2, 1986, pp. 224–225.

[2] Yoon, M. K., Jeon, C. S., and Kauh, S. K., "Efficiency Increase of an Induction Motor by Improving Cooling Performance," *IEEE Transactions on Energy Conversion*, Vol. 17, No. 1, 2002, pp. 1–6. doi:10.1109/60.986430

[3] Nakahama, T., Biswas, D., Kawano, K., and Ishibashi, F., "Improved Cooling Performance of Large Motors Using Fans," *IEEE Transactions on Energy Conversion*, Vol. 21, No. 2, 2006, pp. 324–331. doi:10.1109/TEC.2006.874245

[4] Beier, K. A., and Weir, T. J., "Methods to Reduce Cooling Fan Noise," Society of Automotive Engineers Paper 56C, 1958, pp. 1–9.

[5] Wright, T., Baladi, J. Y., and Hackworth, D. T., "Quiet Cooling System Development for a Traction Motor," American Society of Mechanical Engineers Paper 85-DET-137, 1985, pp. 1–6.

[6] Ghosh, M., "Vibration Analysis of a Rotating Cooling Fan," *Proceedings of the International Modal Analysis Conference & Exhibit*, Vol. 1, Union College, Schenectady, NY, 1985, pp. 459–464.

[7] Szogyen, J. R. M., "Cooling of Electric Motors," *Electric Power Applications*, Vol. 2, No. 2, 1979, pp. 59–67.

[8] Bone, J. C. H., "Cooling and Cooling Circuits for Electric Motors," *Electric Power Applications*, Vol. 1, No. 2, 1978, pp. 37–44.

[9] Lee, Y., Hahn, S., and Kauh, S., "Thermal Analysis of Induction Motor with Forced Cooling Channels," *IEEE Transactions on Magnetics*, Vol. 36, No. 4, 2000, pp. 1398–1402. doi:10.1109/20.877700

[10] Nonaka, S., Yamamoto, M., Nakano, M., and Kawase, M., "Analysis of Ventilation and Cooling System for Induction Motors," *IEEE Transactions on Power Apparatus and Systems*, Vol. PAS-100, No. 11, 1981, pp. 4636–4643. doi:10.1109/TPAS.1981.316805

[11] Hay, N., Lampard, D., Pickering, S. J., and Roylance, T. F., "Convection Heat Transfer Correlations Relevant to Cooling Situations in Electric Motors," American Society of Mechanical Engineers Paper 93-WA/HT-18, 1993, pp. 1–8.

[12] Sapojnikoff, V. G., "Tips on Getting the Most Cooling from the Right Cooling Fan," *Electromechanical Design*, Vol. 16, No. 10, 1972, pp. 18–21.

[13] Khoze, A. N., Beinusov, A. G., and Cherkas, A. Y., "Investigation of Air-Evaporative Cooling of Electric Actuating Motors," *Soviet Electrical Engineering*, Vol. 48, No. 2, 1977, pp. 36–39.

[14] Burmester, J., "Cooling and Noise Behavior of Square-Frame DC Motors in the Low Output Range," *Siemens Power Engineering*, Vol. 3, Nos. 8–9, 1981, pp. 255–259.

[15] Sheu, M. J., "Numerical Investigation of Design Parameters for an Axial Flow Cooling Fan," Society of Automotive Engineers Paper 970933, 1997, pp. 55–64.

[16] Nakahama, T., Suzuki, K., Hashidume, S., Ishibashi, F., and Hirata, M., "Cooling Airflow in Unidirectional Ventilated Open-Type Motor for Electric Vehicles," *IEEE Transactions on Energy Conversion*, Vol. 21, No. 3, 2006, pp. 645–651. doi:10.1109/TEC.2006.877364

[17] Dessouky, Y. G., Williams, B. W., and Fletcher, J. E., "Cooling Enhancement of Electric Motors," *IEE Proceedings. Electric Power Applications*, Vol. 145, No. 1, 1998, pp. 57–60. doi:10.1049/ip-epa:19981472

[18] Farsane, K., Desevaux, P., and Panday, P. K., "Experimental Study of the Cooling of a Closed Type Electric Motor," *Applied Thermal Engineering*, Vol. 20, No. 14, 2000, pp. 1321–1334. doi:10.1016/S1359-4311(99)00094-0

[19] Chen, Y., Chen, B., Chen, C., and Dong, J. Q., "CFD Thermal Analysis and Optimization of Motor Cooling Fin Design," *Proceedings of the ASME Summer Heat Transfer Conference*, Vol. 3, American Society of Mechanical Engineers, New York, 2005, pp. 625–629.

[20] Li, H., "Fluid Flow Analysis of a Single-Stage Centrifugal Fan with a Ported Diffuser," *Engineering Applications of Computational Fluid Mechanics*, Vol. 3, No. 2, 2009, pp. 147–163.